# Designing model imino bifunctional chelators for radiopharmaceuticals – in vitro antitumor activity, photoluminescence and structural analysis†

Alice Brink *[a], Robin E. Kroon [b], Hendrik G. Visser [a], Constance E. J. van Rensburg [c] and Andreas Roodt [a]

[a]Department of Chemistry, University of the Free State, P.O. Box 339, Bloemfontein 9300, South Africa. E-mail: brinka@ufs.ac.za
[b]Department of Physics, University of the Free State, P.O. Box 339, Bloemfontein 9300, South Africa
[c]Department of Pharmacology, University of Pretoria, Basic Medical Sciences Building, 6th floor, 9 Bophelo Road, Prinshof Campus, South Africa

## Abstract

Five imino salicylidene based bifunctional chelators were developed in order to act as a multipurpose ligand system. The chelators, namely 5-methyl-2-(1,2,4-triazol-3-yliminomethyl)phenol, 2-(9-ethylcarbazol-3-yliminomethyl)-5-methylphenol, 2-[(2-imidazol-4-yl)ethyliminomethyl]-5-methylphenol, 2-[(2-indol-3-yl-ethyl)iminomethyl]-5-methylphenol and 2-[2-(4-hydroxyphenyl)ethyliminomethyl]-5-methylphenol, all of which contain a biological directing functional group on the imine moiety, were investigated via crystallographic and DFT structural studies. Synthesis, in vitro cell testing and photoluminescence are reported indicating specific quantum yields and the respective suitability for radiopharmaceutical development.

## 1. Introduction

Considerable interest is expressed in the design of target-specific radiopharmaceuticals whereby the distribution of the agents is determined by the selective receptor binding or other biological interactions.[1] The understanding of the chemical and physical properties of these model radiopharmaceuticals therefore becomes essential. The trend of radiometal complexes synthesized for this purpose often contains a receptor ligand known as a targeting biomolecule which is coordinated to the radionuclide via a chelator or a linker. A bifunctional chelator serves the primary function of joining this biomolecule to the transition metal complex. The selection of the bifunctional chelator is largely determined by the nature and oxidation state of the transition metal under consideration. Several excellent ligand systems have been suggested as possible bifunctional chelators particularly for use with fac-$[M(CO)_3(H_2O)_3]^+$ complexes (M = Mn, Tc, Re).[2–9] Our research group focuses on the use of bidentate ligands (L,L′-Bid) for use in catalysis and radiopharmaceutical drug design, utilizing the [2 + 1] method.[10–13] This approach holds significant potential especially in view of recent reports whereby proteins coordinate to fac-$[Re(CO)_3]^+$ followed by selective mono- or bidentate ligand coordination.[14–16] A range of mono-negative bidentate ligands, (L,L′-Bid), were designed by us and reported herein. The ligand systems allow convenient coordination of selected aromatic, aliphatic or biologically active molecules to a common coordinative backbone derived from the salicylaldehyde starting reagent. The advantage of the imino bifunctional chelators are the ease and purity of the final compound as well as its manipulable character. Parameters such as steric and electronic properties, donor atoms, chirality, denticity and biological functions can readily be altered and optimized. As our interest

focuses on the possible effects which the different molecules, coordinated to the backbone of the bidentate ligand, would have on the fac-$[Re(CO)_3]^+$ metal centre, this has thus led to kinetic studies of the mechanism of substitution and activation parameters of fac-[Re(L,L′-Bid)$(CO)_3$(S)] (S = monodentate ligands) complexes.[12,13] The span of activation introduced by the set of bidentate ligands utilized is of particular importance, as it allows us to estimate the effects introduced on primary and secondary in vivo activity due to the metal centre activation/de-activation reaction. The structural characteristics of such ligand systems are therefore essential for understanding the chemical and biological activities of the final fac-[Re(L,L′-Bid)$(CO)_3$(S)] complexes. Therefore the following series of imino bifunctional chelators containing a vast range of biologically active functional groups were explored and consist of 1,2,4-triazole, 3-amino-carbazole, histamine, tryptamine and tyramine functionalities. The biological applications of the functional groups vary and include the 1,2,4-triazole which is the basis of modern agricultural fungicides as well as drugs for fungal diseases in humans.[17] 3-Amino-9-ethylcarbazole is used to detect cytochrome oxidase[18] and in staining kits for immunohistochemistry.[19] Histamine binds to the H1 receptor and causes allergic and hypersensitivity reactions.[20] Tryptamine contains an indole ring structure and is classified as a neurotransmitter.[21] Tyramine is a biogenetically related catecholamine, a chemical class of neurotransmitters produced by the adrenergic system.[22] The chelators, containing various functional groups, were designed as multi-purpose ligand systems with the potential of achieving several aims such as the coordination to the radiopharmaceutical synthon, fac-$[M(CO)_3]^+$; possible chemotherapeutic application by containing a biological directing molecule and finally as a biological cellular imaging agent with photoluminescent properties. Structurally, they exhibit systematic variations and contain aromatic functionalities varying in size either directly coordinated to the imine nitrogen atom or displaced further from the rhenium metal center by an ethylimino chain (Fig. 1). Single crystal X-ray diffraction, computational DFT calculations, in vitro antitumor activities and photoluminescence results of these chelators are reported herein.

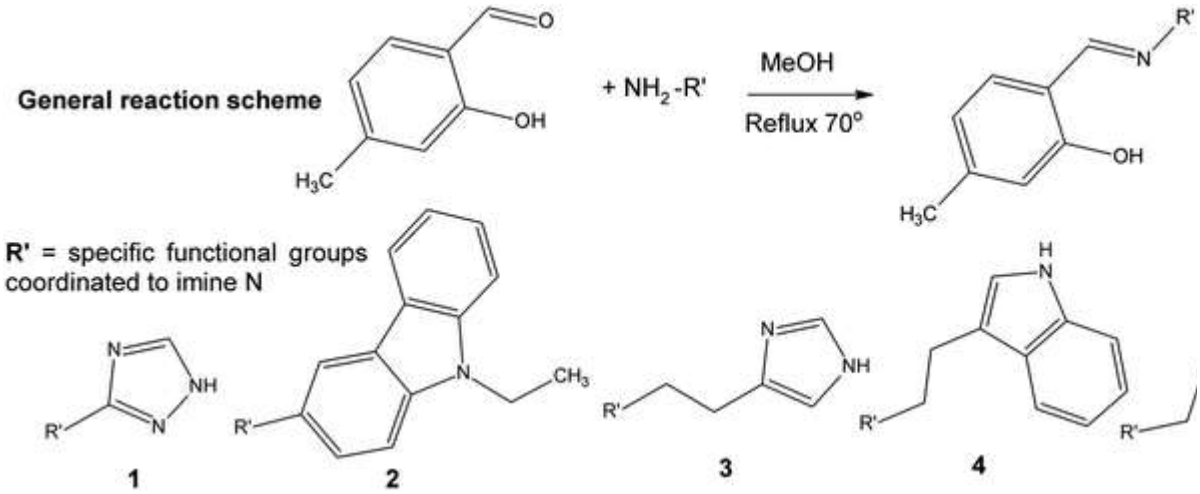


**Fig. 1** The chemical formation and general structure of compounds **1**–**5**.

## 2. Experimental details

### 2.1 Materials and measurements

All experiments were performed anaerobically under Schlenk conditions using double distilled water and methanol. Schlenk conditions were utilised to improve yields and for safety purposes as certain reagents (i.e. histamine) can cause anaphylactic shock. Unless otherwise stated, all chemicals were of reagent grade and purchased from Sigma Aldrich. Elemental analysis was performed on a LECO Truspec Micro Elemental Analyzer. The $^{1}H$ and $^{13}C$ FT-NMR spectra were recorded at 600.28 and 150.96 MHz respectively on a Bruker AXS 600 MHz at 25 °C; for $^{1}H$: in $CD_3OD$ (3.31 ppm), $C_3H_6O$ (2.05 ppm) and $CDCl_3$ (7.26 ppm); and $^{13}C$: in $CD_3OD$ (49.0 ppm), $C_3H_6O$ (29.8 ppm) and $CDCl_3$ (77.2 ppm). Chemical shifts are reported in ppm and referenced to solvent signals as indicated. The molecular structure of compounds **1–5** is indicated in Fig. 2.

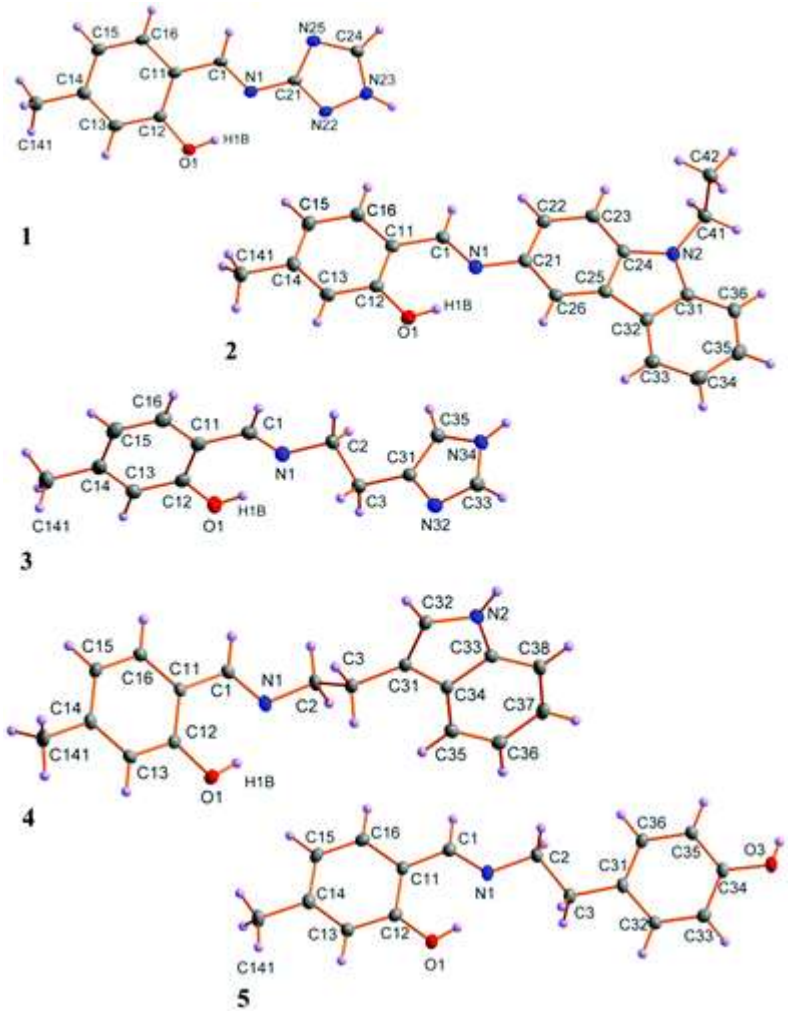


**Fig. 2** Molecular structures of compounds **1–5** indicating atom numbering scheme. Hydrogen atoms are drawn as spheres of arbitrary radius. Compounds **3** and **5** contain two molecules in the asymmetric unit. Atom numbering for these respective molecules are found in the ESI† (Fig. S1).

## 2.2 Synthesis

2.2.1 Preparation of 5-methyl-2-(1,2,4-triazol-3-yliminomethyl)phenol (**1**). The title compound was synthesized by the slow addition of 3-amino-1,2,4-triazole (0.309 g, 3.67 mmol) dissolved in methanol, to 2-hydroxy-4-methyl benzaldehyde (0.500 g, 3.67 mmol) (cooled to 0 °C). The reaction was gradually heated to room temperature and then stirred at 70 °C for 3 h. The product was obtained as a pale yellow solid. The solid was washed with cold methanol and filtered. Crystals suitable for X-ray diffraction were obtained by the slow evaporation of the filtrate (yield: 0.608 g, 82%). Anal. calcd: C, 59.40; H, 4.98; N, 27.71. Anal. found: C, 60.0; H, 5.10; N, 28.88. $^{1}$H NMR (600 MHz, acetone-$d_6$) δ 9.37 (s, 1H, HC=N), 7.56 (d, 1H, J = 7.9 Hz), 6.85 (d, 1H, J = 7.9 Hz), 6.82 (s, 1H), 3.30 (s, 1H), 2.36 (s, 3H, $CH_3$). $^{13}$C NMR (151 MHz, acetone-$d_6$) δ 167.05, 146.37, 134.42, 121.47, 118.10, 117.39, 21.87.

2.2.2 Preparation of 2-(9-ethylcarbazol-3-yliminomethyl)-5-methylphenol (**2**). The title compound was synthesized according to the procedure described in Section 2.2.1, using 2-hydroxy-4-methyl benzaldehyde (1.00 g, 7.35 mmol) and 3-amino-9-ethyl-carbazole (1.54 g, 7.35 mmol) in methanol under Schlenk conditions. The product was obtained as a yellow solid which was washed with cold methanol and filtered. Crystals suitable for X-ray diffraction were grown from a methanol : acetone : benzene (6 : 2 : 1) solution at 4 °C (yield: 2.15 g, 90%). Anal. calcd: C, 80.46; H, 6.14; N, 8.53. Anal. found: C, 81.12; H, 6.14; N, 7.71. $^{1}$H NMR (600 MHz, acetone-$d_6$) δ 13.57 (s, 1H, OH), 9.01 (s, 1H, HC=N), 8.26 (m, 1H), 8.21 (d, 1H, J = 7.8 Hz), 7.64 (d, 1H, J = 8.6 Hz), 7.61–7.59 (m, 2H), 7.51–7.47 (m, 2H), 7.24 (m, 1H), 6.81 (m, 2H), 4.51 (q, 2H, J = 7.2 Hz, $CH_2$), 2.35 (s, 3H, $CH_3$), 1.42 (t, 3H, J = 7.2 Hz, $CH_3$). $^{13}$C NMR (151 MHz, acetone-$d_6$) δ 161.97, 161.43, 144.21, 141.57, 141.30, 139.96, 133.07, 127.00, 124.40, 123.77, 121.43, 120.85, 120.65, 119.89, 118.41, 117.88, 113.55, 110.31, 110.00, 38.19, 21.99, 14.10.

2.2.3 Preparation of 2-[(2-imidazol-4-yl)ethyliminomethyl]-5-methylphenol (**3**). The title compound was synthesized according to the procedure described in Section 2.2.1, using 2-hydroxy-4-methyl benzaldehyde (0.500 g, 3.67 mmol) and histamine (0.408 g, 3.67 mmol) dissolved in methanol under Schlenk conditions. Crystals suitable for X-ray diffraction were grown from methanol at 5 °C (yield: 0.808 g, 96%). Anal. calcd: C, 68.10; H, 6.59; N, 18.33. Anal. found: C, 68.27; H, 6.46; N, 18.92. $^{1}$H NMR (600 MHz, acetone-$d_6$) δ 8.38 (s, 1H, HC=N), 7.53 (s, 1H), 7.20 (d, 1H, J = 7.9 Hz), 6.84 (s, 1H), 6.69 (s, 1H), 6.68 (s, 1H), 3.87 (t, 2H, J = 7.0 Hz), 2.94 (t, 2H, J = 7.0 Hz), 2.29 (s, 3H, $CH_3$). $^{13}$C NMR (151 MHz, acetone-$d_6$) δ 166.31, 162.20, 143.52, 135.49, 132.22, 121.96, 120.23, 117.74, 117.64, 59.80, 22.04, 21.68.

2.2.4 Preparation of 2-[(2-indol-3-yl-ethyl)iminomethyl]-5-methylphenol (**4**). The title compound was synthesized according to the procedure described in Section 2.2.1, using 2-hydroxy-4-methyl benzaldehyde (1.00 g, 7.35 mmol) and tryptamine (1.18 g, 7.35 mmol) dissolved in methanol under Schlenk conditions (yield: 1.71 g, 84%). Anal. calcd: C, 77.67; H, 6.52; N, 10.06. Anal. found: C, 79.42; H, 6.42; N, 8.68. $^{1}$H NMR (600 MHz, acetone-$d_6$) δ 13.48 (s, 1H, OH), 8.36 (s, 1H, HC=N), 7.63 (d, 1H, J = 7.8 Hz), 7.37 (dt, 1H, J = 0.8, 8.1 Hz), 7.17 (m, 2H), 7.09 (dq, 1H, J = 1.0, 7.0 Hz), 7.02 (dq, 1H, J = 1.0, 7.0 Hz), 6.70 (s, 1H), 6.67 (d, 1H, J = 7.8 Hz), 3.91 (dt, 2H, J = 1.0, 7.0 Hz), 3.14 (dt, 2H, J = 1.0, 7.0 Hz), 2.29 (s, 3H, $CH_3$). $^{13}$C NMR (151 MHz, acetone-$d_6$) δ 166.17, 162.23, 143.49, 137.68, 132.18, 128.45, 123.59, 122.09, 120.21, 119.43, 119.26, 117.73, 117.60, 113.38, 112.16, 60.59, 27.77, 21.68.

2.2.5 Preparation of 2-[2-(4-hydroxyphenyl)ethyliminomethyl]-5-methylphenol (**5**). The title compound was synthesized according to the procedure described in Section 2.2.1, using 2-hydroxy-4-methyl benzaldehyde (0.500 g, 3.67 mmol) and tyramine (0.504 g, 3.67 mmol) (yield: 0.851 g, 91%). Anal. calcd: C, 75.27; H, 6.71; N, 5.49. Anal. found: C, 76.96; H, 6.50;

N, 5.21. $^{1}$H NMR (600 MHz, acetone-$d_6$) δ 8.34 (s, 1H, HC=N), 7.19 (d, 1H, J = 8.5 Hz), 7.07 (dt, 2H, J = 2.1, 2.8, 8.5 Hz), 6.74 (dt, 2H, J = 2.1, 2.8, 8.5 Hz), 6.69 (d, 2H, J = 7.5 Hz), 3.79 (dt, 2H, J = 1.2, 7.5 Hz), 2.89 (t, 2H, J = 7.5 Hz), 2.28 (s, 3H, $CH_3$). $^{13}$C NMR (151 MHz, acetone-$d_6$) δ 166.29, 162.13, 156.68, 143.54, 132.20, 131.09, 130.70, 120.25, 117.71, 117.54, 115.97, 61.90, 37.26, 21.67.

### 2.3 Determination of X-ray crystal structures

Diffraction data for **1–5** were collected using a Bruker X8 ApexII 4K diffractometer[23] using Mo Kα radiation with ω-and-φ-scans at 100 K. COSMO[24] was utilized for optimum collection of more than a hemisphere of reciprocal space. Frame integration and data reduction were performed using the Bruker SAINT-Plus and XPREP[25] software packages, respectively. Data were corrected for absorption effects using the multi-scan technique SADABS.[26] The structures were solved using the direct methods package SIR97[27] and refined using the software package WinGX,[28] incorporating SHELXL.[29] All non-hydrogen atoms were refined with anisotropic displacement parameters, while the methyl, methylene and aromatic H atoms were placed in geometrically idealized positions and constrained to ride on their parent atoms, with (C–H = 0.98–0.95 Å and $U_{iso}$(H) = 1.5$U_{eq}$(C) and 1.2$U_{eq}$(C)), respectively. The methyl protons were located from a difference Fourier map and the group was refined as a rigid motor. The absolute structure parameter for compounds **1** and **2** has been removed from the CIF file. The s.u. of the Flack parameter is large (greater than or equal to 0.3), (Flack parameter of **1** is 0(2) and of **2** is 1.9(15)) thus preventing the absolute structure from being determined from the data. The compounds are weak anomalous scatters and therefore the absolute structure parameter is considered meaningless. The program DIAMOND[30] was used for all graphical representation of the crystal structures. All structures are shown with thermal ellipsoids drawn at 50% probability level unless otherwise stated. Graphical representations of overlays of selected complexes are obtained with Hyperchem 7.52.[31] The crystal data and structural refinement parameters are listed in Table 1. Geometrical parameters of interest to specific bond angles and distances are listed in Table 2.

**Table 1** Crystal data and structural refinement parameters

| **Compound** | **1** | **2** | **3** | **4** | **5** |
|---|---|---|---|---|---|
| Empirical formula | $C_{10}H_{10}N_4O$ | $C_{22}H_{20}N_2O$ | $C_{13}H_{15}N_3O$ | $C_{18}H_{18}N_2O$ | $C_{16}H_{17}NO_2$ |
| Formula weight | 202.22 | 328.40 | 229.28 | 278.34 | 255.31 |
| Temperature (K) | 100(2) | 100(2) | 100(2) | 100(2) | 100(2) |
| Wavelength (Å) | 0.71073 | 0.71073 | 0.71073 | 0.71073 | 0.71073 |
| Crystal system | Orthorhombic | Orthorhombic | Monoclinic | Triclinic | Triclinic |
| Space group | $Pca2_1$ | $P2_12_12_1$ | $P2_1/c$ | $P\bar{1}$ | $P\bar{1}$ |
| Unit cell dimensions | | | | | |
| a (Å) | 21.079(3) | 7.9040(2) | 10.4959(3) | 6.0722(3) | 7.3079(5) |
| b (Å) | 4.4677(5) | 10.5709(3) | 9.9047(3) | 8.3073(3) | 11.7966(8) |
| c (Å) | 10.0801(12) | 20.3219(6) | 23.1897(6) | 14.1215(6) | 15.5593(11) |
| α (°) | 90 | 90 | 90 | 98.482(2) | 89.413(4) |
| β (°) | 90 | 90 | 106.365(2) | 96.914(2) | 77.258(3) |

| **Compound** | **1** | **2** | **3** | **4** | **5** |
|---|---|---|---|---|---|
| γ (°) | 90 | 90 | 90 | 94.487(2) | 80.098(4) |
| Volume ($Å^3$) | 949.3(2) | 1697.94(8) | 2313.10(11) | 696.07(5) | 1288.28(15) |
| Z | 4 | 4 | 8 | 2 | 4 |
| Crystal colour | Colourless | Yellow | Yellow | Yellow | Yellow |
| Crystal morphology | Needle | Plate | Cuboid | Plate | Needle |
| Crystal size (mm) | 0.39 × 0.06 × 0.04 | 0.40 × 0.18 × 0.06 | 0.41 × 0.17 × 0.14 | 0.39 × 0.12 × 0.07 | 0.33 × 0.09 × 0.08 |
| Theta range (°) | 3.87 to 28.00 | 3.22 to 28.00 | 3.19 to 27.99 | 2.68 to 28.00 | 1.34 to 28.00 |
| Completeness (%) | 99.5 | 99.8 | 99.8 | 99.4 | 98.3 |
| Index ranges | h = −27 to 27 | h = −10 to 7 | h = −13 to 13 | h = −7 to 8 | h = −9 to 9 |
| | k = −5 to 3 | k = −13 to 13 | k = −13 to 13 | k = −10 to 10 | k = −15 to 15 |
| | l = −13 to 13 | l = −26 to 26 | l = −30 to 29 | l = −18 to 18 | l = −20 to 20 |
| Reflections collected | 11 211 | 30 092 | 23 821 | 12 530 | 24 644 |
| Independent reflections | 1201 | 2344 | 5567 | 3315 | 6114 |
| $R_{int}$ | 0.0572 | 0.0323 | 0.0435 | 0.0243 | 0.0415 |
| Data/restraints/parameters | 1201/1/137 | 2344/0/230 | 5567/0/311 | 3315/0/192 | 6114/0/345 |
| Goodness-of-fit on $F^2$ | 1.125 | 1.049 | 1.043 | 1.074 | 1.086 |
| Final R indices [I > 2σ(I)] | $R_1$ = 0.0427, $wR_2$ = 0.1022 | $R_1$ = 0.0333, $wR_2$ = 0.0858 | $R_1$ = 0.0449, $wR_2$ = 0.1023 | $R_1$ = 0.0436, $wR_2$ = 0.1148 | $R_1$ = 0.0547, $wR_2$ = 0.1445 |
| R indices (all data) | $R_1$ = 0.0515, $wR_2$ = 0.1080 | $R_1$ = 0.0366, $wR_2$ = 0.0884 | $R_1$ = 0.0700, $wR_2$ = 0.1151 | $R_1$ = 0.0518, $wR_2$ = 0.1222 | $R_1$ = 0.0776, $wR_2$ = 0.1629 |
| $\rho_{max}$ and $\rho_{min}$ (e $Å^{-3}$) | 0.395 and −0.401 | 0.208 and −0.226 | 0.236 and −0.235 | 0.393 and −0.400 | 0.787 and −0.691 |

**Table 2** Selected geometrical parameters of the presented functionalized imino salicylidene based chelators, tabulated for comparison [Å and °]

| **Compound** | **(1)** | **(2)** | **(3)** | | **(4)** | **(5)** | |
|---|---|---|---|---|---|---|---|
| Molecule | | | **1** | **2** | | **1** | **2** |
| Bonds distance (Å) | | | | | | | |
| N1–C1 | 1.294(3) | 1.290(2) | 1.282(2) | 1.280(2) | 1.282(2) | 1.296(2) | 1.298(2) |
| N1–C2/C5 | — | — | 1.459(2) | 1.461(2) | 1.462(1) | 1.464(2) | 1.461(2) |
| N1–C21 | 1.388(3) | 1.422(2) | — | — | — | — | — |
| C1–C11 | 1.440(4) | 1.453(2) | 1.453(2) | 1.455(2) | 1.462(2) | 1.415(2) | 1.415(2) |
| C12–O1 | 1.348(3) | 1.355(2) | 1.357(2) | 1.362(2) | 1.346(2) | 1.296(2) | 1.297(2) |
| N1···H1B | 1.863(2) | 1.864(1) | 1.856(1) | 1.866(2) | 1.827(1) | 1.809(2) | 1.884(1) |
| Bond angle (°) | | | | | | | |
| O1–C12–C11 | 121.6(2) | 121.7(1) | 121.4(1) | 121.1(1) | 121.6(1) | 120.9(2) | 120.9(2) |
| N1–C1–C11 | 121.3(2) | 121.2(1) | 122.0(1) | 122.2(1) | 120.9(1) | 122.5(2) | 123.9(2) |
| C1–N1–C2/C5 | — | — | 117.9(2) | 118.3(1) | 118.5(1) | 125.4(2) | 124.9(2) |
| C1–N1–C21 | 120.0(2) | 122.6(1) | — | — | — | — | — |
| N1–C2–C3 | — | — | 109.6(1) | 110.9(1) | 107.0(1) | 107.5(1) | 111.1(2) |
| Torsion angle (°) | | | | | | | |
| O1–C12–C11–N1 | 1.7(3) | 3.1(2) | 1.6(2) | 1.4(2) | 2.5(1) | 3.2(2) | 6.5(2) |
| C1–N1–C21–C22 | 1.5(4) | 0.6(2) | — | — | — | — | — |
| C1–N1–C2–C3 | — | — | 114.8(1) | 134.8(1) | 103.9(1) | 173.1(2) | 129.9(2) |
| Dihedral angle through ring 1 and ring 2 (°) | 4.58(8) | 4.37(4) | 77.25(5) | 77.70(5) | 48.44(3) | 10.43(5) | 59.00(6) |

### 2.4 Computational details

Computational calculation results were obtained using the GAUSSIAN-03W[32] software package. DFT calculations were performed at the B3LYP[33] level of theory with the 6-31G++(d,p)[34,35] basis set for the main group elements, using the High Performance Computing Facility of the University of the Free State. Optimized structures were verified as minima through frequency analysis. The crystal structures are denoted with numerical values, for example 5-methyl-2-(1,2,4-triazol-3-yliminomethyl)phenol is indicated as **1**. The corresponding optimized structures is indicated as **1*** respectively.

### 2.5 In vitro antitumor activity evaluation by SRB assays

The human cell lines TK10 (renal), UACC62 (melanoma) and MCF7 (breast) were obtained from the National Cancer Institute (NCI) in the framework of a collaborative research program between the Council for Scientific and Industrial Research (CSIR) and NCI. The three cell line panels are recommended by the National Cancer Institute for preliminary screens. The SRB assay, for this study, was performed by the Council for Scientific and Industrial Research, South Africa,[36,37] in accordance with the protocol of the Drug Evaluation Branch of the National Cancer Institute. The SRB assay protocol is described in the ESI.†

### 2.6 Determination of photoluminescence

The measurements were made using an Edinburgh Instruments FLS980 photoluminescence spectrometer with double monochromators. Solid state powdered samples were excited by a 450 W xenon lamp and the luminescence was measured using a Hamamatsu R928P photomultiplier tube. The inset images of the emission were photographed using a Nikon Coolpix E8400 digital camera. All spectra were corrected for the spectral response of the system. The quantum yield was measured using an integrating sphere. The total excitation light was recorded using a reflective Spectralon sample, after which the excitation light reflected from the sample and the luminescence was measured under identical conditions. The luminescence output (integrated area under the emission curve) was divided by the absorbed light (integrated difference of the reflection from the Spectralon and the sample) to give the quantum yield.

## 3. Results and discussion

### 3.1 Synthesis

The compounds were synthesized from the reactions of 2-hydroxy-4-methyl benzaldehyde and various biologically active amines[38–41] according to the previously reported methods.[42,43] Single crystals suitable for X-ray diffraction were obtained from methanol or methanol–acetone–benzene solvent mixtures at 4 °C. All compounds were isolated as the trans phenol-imine (O–H···N) tautomeric form. Temperature studies to induce the crystallization of the cis and/or the keto-amine isomer were unsuccessful.[44] All compounds indicate the imine hydrogen atom in $^{1}$H NMR at ca 9.3–8.3 ppm as well as the imine carbon atom in $^{13}$C NMR at ca. 167–162 ppm. Compounds on average were characterized in deuterated acetone as the use of chlorinated solvents lead to the appearance of rotamers as identified by $^{1}$H NMR. Optimal yields were obtained under Schlenk conditions and compounds were stable for several months under an argon atmosphere.

### 3.2 Single crystal structure analysis

All the five iminophenol compounds contain biological functionalities linked to a common salicylaldehyde backbone. The molecules of compounds **1** to **5** crystallize in the trans phenol-imine tautomeric form with strong intramolecular hydrogen bonds between the O–H···N atoms (Fig. 2, Table 2 and Tables S1–S5, ESI†). Compounds **1** and **2** have an aromatic functionality bonded directly to the imine N atoms. These ligands crystallize in orthorhombic crystal systems with space groups of $Pca2_1$ and $P2_12_12_1$ respectively. The ligands show a planar orientation (Fig. 3a and Table 2) with a minimal rotation around the C1=N1 double bond, despite the relatively large size of the carbazole functionality in **2** (a 13 member aromatic ring system) versus the five membered ring system in **1** (Fig. 3a).

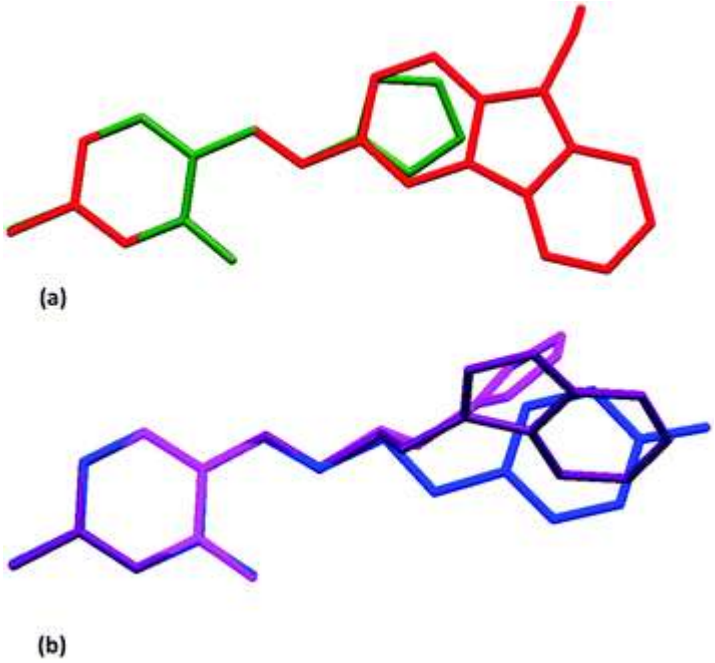


**Fig. 3** (a) Graphical overlay of structures **1** (green) and **2** (red) to illustrate similarly in the aromatic ring orientation. Overlay drawn through atoms O1, N1, C1, C11, C12, C13, C14, C15, and C16 of respective compounds to allow free rotation of coordinated functionalities. (b) Graphical overlay of structures **3** (violet), **4** (purple) and **5** (blue) illustrating variations in the orientation of the imine functionality.

The salicylidene compounds **3**, **4** and **5** all have a $–CH_2CH_2–R$ chain bonded to the N atom of the salicylaldehyde backbone, where R = aromatic functionalities such as histamine, tryptamine and tyramine. None of these molecules are planar (Fig. 3b) as indicated by the dihedral angles drawn through the aromatic backbone of C11, C12, C13, C14, C15, and C16 and the plane drawn through the imine aromatic functionality (Table 2). Interestingly compound **5**, which contains two independent molecules in the asymmetric unit, has one molecule that is more planar than the other indicated by the dihedral angles of 10.43(5)° versus 59.00(6)° (Fig. S2, ESI†). Compound **3**, also containing two molecules in the asymmetric unit, both have similar dihedral angles of 77.25(5)° and 77.70(5)° respectively. Molecules **4** and **5** crystallise in the same space group $P\bar{1}$, showing significant variations in the unit cell parameters attributed to the different substituents.

### 3.3 Optimized geometry

The DFT optimized calculations were computed to obtain additional insight into the solid state structures in an attempt to explain the bonding nature, planarity and flexibility of five organic systems as the basic backbone of the compound, 5-methyl-2-(x-yliminomethyl)phenol, is utilised as a bifunctional chelator which can be easily functionalised and adjusted.[13,45,46] The structural differences between the solid state and the theoretical optimized structures are graphically represented by overlay diagrams and can be mathematically described by the root mean square (RMS) value, which is a measure of how far the average is from zero, providing information on the variations of bond lengths and angles. A fairly good correlation was obtained between the optimized structures (drawn in red) and the experimental solid state structures (blue) as indicated qualitatively (Fig. 4 and Fig. S4–S7, ESI†) which represents the superimposed image of complexes on those of the optimized counterparts. The RMS values are listed in each figure caption. All optimised

structures indicate the phenol-imine tautomeric form with no H-atom transfer to the keto-amine isomer, which is in agreement with the crystallographic data. A comparison of geometric parameters for all five compounds can be found in Table 3 whereby the crystal structure is compared to the optimised DFT structure.

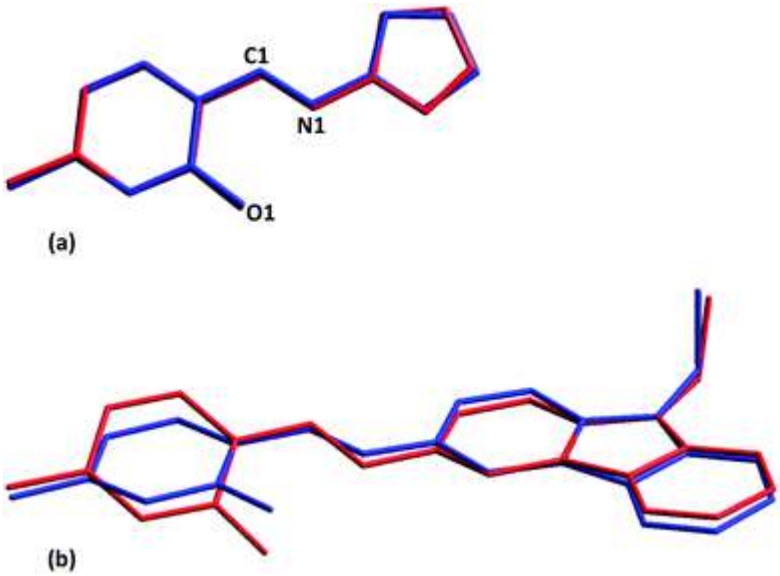


**Fig. 4** (a) Graphical representation of the overlay of the DFT optimized structure **1*** (red) with the crystal structure of **1** (blue) (RMS value = 0.095 Å). (b) The overlay of crystal structure **2** (blue) and DFT optimized structure **2*** (red) (RMS value = 0.372 Å). Overlay fit excludes all hydrogen atoms.

**Table 3** Comparison of selected ligand geometrical parameters of crystal structures **1–5** with the optimized structure **1*–5*** [Å and °]

| | **1** Crystal | **1*** DFT | **2** Crystal | **2*** DFT | **3** Crystal molecule 1 | **3** Crystal molecule 2 | **3*** DFT |
|---|---|---|---|---|---|---|---|
| N1–C1 | 1.294(4) | 1.294 | 1.290(2) | 1.289 | 1.282(2) | 1.280(2) | 1.282 |
| N1–C21 | 1.388(3) | 1.383 | 1.422(2) | 1.409 | — | — | — |
| N1···O1 | 2.605(3) | 2.631 | 2.607(2) | 2.634 | 2.600(2) | 2.610(2) | 2.631 |
| C1–C11 | 1.440(1) | 1.442 | 1.453(2) | 1.449 | 1.453(2) | 1.455(2) | 1.454 |
| O1–C12 | 1.348(3) | 1.339 | 1.355(2) | 1.342 | 1.357(2) | 1.362(2) | 1.342 |
| C11–C1–N1 | 121.3(2) | 121.78 | 121.2(1) | 122.4 | 122.0(1) | 122.2(1) | 122.8 |
| O1–C12–C11 | 121.6(2) | 122.10 | 121.7(1) | 121.7 | 121.4(2) | 121.1(1) | 121.7 |
| C1–N1–C21 | 120.0(2) | 119.64 | 122.6(1) | 122.0 | — | — | — |
| O1–C12–C11–N1 | 1.7(3) | 0 | 3.1(2) | 0.122 | 1.6(2) | 1.4(2) | 0.01 |
| Dihedral angle between aromatic rings | 4.58(8) | 0.2 | 4.37(4) | 32.5 | 77.25(5) | 77.70(5) | 3.83 |

| | **4** Crystal | **4*** DFT | **5** Crystal molecule 1 | **5** Crystal molecule 2 | **5*** DFT |
|---|---|---|---|---|---|
| N1–C1 | 1.282(2) | 1.282 | 1.296(2) | 1.298(2) | 1.282 |
| N1–C21 | — | — | — | — | — |
| N1···O1 | 2.574(2) | 2.635 | 2.566(2) | 2.627(2) | 2.635 |
| C1–C11 | 1.462(2) | 1.454 | 1.415(2) | 1.41(2) | 1.453 |
| O1–C12 | 1.346(2) | 1.342 | 1.296(2) | 1.297(2) | 1.342 |
| C11–C1–N1 | 120.9(1) | 122.9 | 122.5(2) | 123.9(2) | 122.9 |
| O1–C12–C11 | 121.6(1) | 121.7 | 120.9(2) | 120.9(2) | 121.7 |
| C1–N1–C21 | — | — | — | — | — |
| O1–C12–C11–N1 | 2.5(1) | 0.04 | 3.2(2) | 6.5(2) | 0.08 |
| Dihedral angle between aromatic rings | 48.44(3) | 45.9 | 10.43(5) | 59.00(6) | 35.7 |

All solid state bond distances listed in Table 3 are comparable to the respective optimised counterparts. A result which has been observed for the chelators bound to fac-$[Re(CO)_3]^+$.[43,47] A notable exception is that of the N···O distance which is shorter (within esd) compared to that of the optimised structures. A phenomenon caused by the intramolecular hydrogen bond experienced in each crystal structure between atoms O1–H···N1. Further structural deviations can be found in the dihedral angles formed by planes drawn through the 5-methyl-2-(x-yliminomethyl)phenol backbone and the functionalised imine aromatic moiety. The various packing effects and atomic interactions found within the crystalized structure explains the orientation of the coordinated substituent relative to the optimized structure. The crystallographic and optimised structure of **1** is both planar with a near zero RMS value. Compound **2** is crystallographically planar despite containing a sterically large 13-membered aromatic ring system. The optimised structure however shows significant twisting of the aromatic rings (the dihedral angle of 4.37(4)° for **2**vs. 32.5° for **2***) (Fig. 4).

The solid state structures of **1** and **2** both have well defined herring-bone packing in the unit cell. Structure **1** has near perpendicular orientation (Fig. 5) of the molecules positioned relative to that at symmetry operator x, y, and z due to the cumulative effects of intermolecular hydrogen bonding, C–H···π interactions and soft N···N interactions as listed in the ESI† (Table S1).

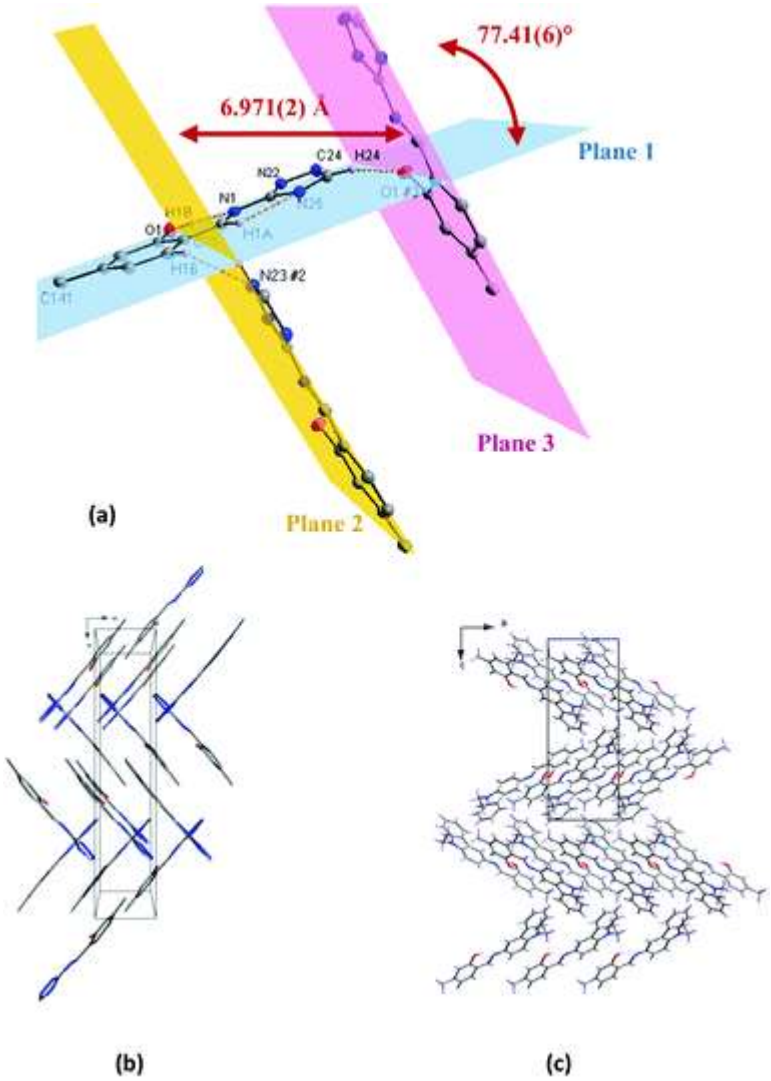


**Fig. 5** (a) Graphical representation for compound **1** of intra- and intermolecular bonding with a near perpendicular orientation of molecules. Hydrogen bonding indicated by orange dotted lines. H atoms are omitted for clarity. (b) Molecular packing of the unit cell as viewed along the c-axis for compound **1**. (c) Molecular packing of compound **2** in the unit cell as viewed along the b-axis.

Structure **2** similarly has extensive π–π interactions and C–H···π interactions between the aromatic 13-membered carbazole ring and the phenol ring all of which will stabilise the relative planarity of the two ring systems in the crystalline state (Fig. S3 and Table S2, ESI†).

The optimised structure of **3*** indicates a predicted degree of planarity due to the dihedral angle of 3.83° (Fig. S4, ESI†). However both structures **3** and **4** show multiple N–H···N, N–H···C/O C–H···π between relative molecules to form infinite one dimensional chains along the [010] vector for **3** as well as having cage-like structures of **4** with respective dihedral angles of 77.25(5)°, 77.70(5)° (for molecules **1** and **2** of structure **3**) and 48.44(3)° for structure **4** (Fig. S4 and S5, ESI†). The dihedral angle of the optimised structure of **5*** (35.7°) is a close mean to the dihedral angles of the two molecules of **5** (10.43(5)° and 59.00(6)°) which are found in the asymmetric unit (Fig. S6 and S7, ESI†).

### 3.4 In vitro cancer cell screen

The cancer in vitro growth inhibitory effects of the imino salicylidene bifunctional chelators were investigated as the ultimate use of these organic ligand systems is the coordination to fac-$[M(CO)_3]^+$ (M = Re and Tc) as a radiopharmaceutical model.[47] The compounds were tested in the 3-cell line panel consisting of TK10 (renal), UACC62 (melanoma) and MCF7 (breast) cancer cells using a Sulforhodamine B (SRB) assay as developed by Skehan et al.[48] to measure drug-induced cytotoxicity and cell proliferation for large-scale drug screening applications.

The growth inhibitory effects of selected compounds are listed in Table 4. Graphical representations of the results are listed in Fig. 6. The percentage (%) growth is the total growth of cells in the treated wells relative to untreated controls over a forty-eight hour experimental period. A 100% growth indicates that there are the same amounts of cells in treated wells as in untreated control wells, after 48 h. Zero percent growth indicates that no increase in cell number (i.e. growth retardation) and negative one hundred percent (−100%) growth indicates that no cells remain after the 48 h of incubation period. The results from the sulforhodamine B assay indicate that no toxicity with respect to the cell lines were found for the selected compounds **1**–**5**. Minimal growth retardation was found for the interaction of **4** with breast MCF7 cells. This therefore indicates that the organic ligand systems have no chemo-therapeutic activity to these specific cancer lines within themselves. Any cancer cell death, which may occur when the compounds are coordinated to the fac-$[M(CO)_3]^+$ core will therefore be due to radioactivity and not from ligand chemotherapeutic effects.

**Table 4** Net growth of renal, melanoma and breast cancer cells analysed according a sulforhodamine B assay against selected compounds

| Compound | Conc. (μM) | Renal cells TK10 growth (%) | Melanoma cells UACC62 growth (%) | Breast cells MCF7 growth (%) |
|---|---|---|---|---|
| **1** | 10 | 79.60(1) | 101.65(8) | 76.15(1) |
| **2** | 10 | 81.08(2) | 101.45(2) | 77.07(5) |
| **3** | 10 | 76.25(1) | 100.58(2) | 82.14(8) |
| **4** | 10 | 86.47(1) | 93.31(2) | 68.63(2) |
| **5** | 10 | 71.83(2) | 97.27(5) | 83.77(2) |
| Emetine (positive control) | 10 | −61.980(2) | −94.230(5) | −47.24(1) |

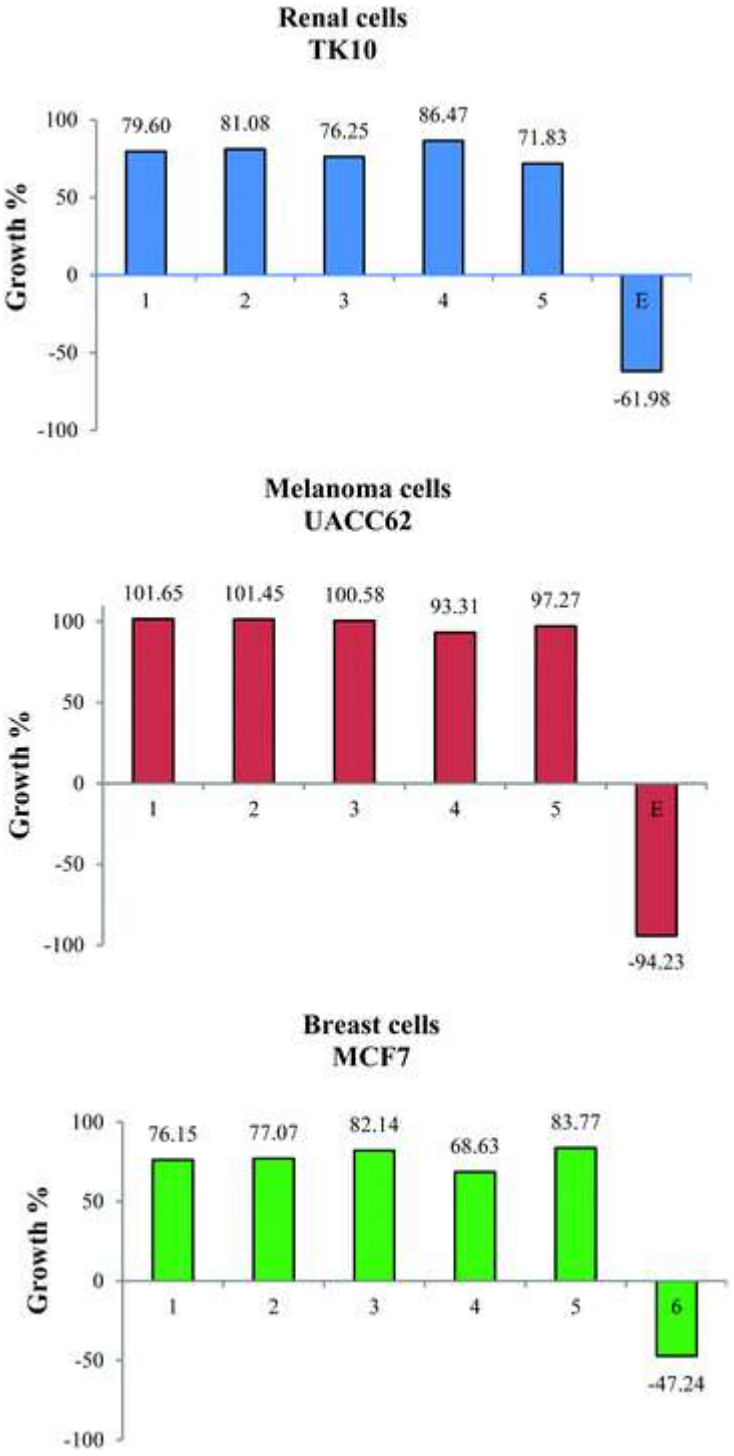


**Fig. 6** Graphical representation of the net growth of renal, melanoma and breast cancer cells analysed according a sulforhodamine B assay against selected compounds.

### 3.5 Photoluminescence results

The imino bifunctional chelators were designed with the potential of achieving several aims such as the coordination to the radiopharmaceutical synthon, fac-$[M(CO)_3]^+$; possible chemotherapeutic application by containing a biological directing molecule and finally as a biological cellular imaging agent. Hence the photoluminescent capability of each organic ligand was investigated.

The spectral properties of compounds **1** and **2** are indicated in Fig. 7 and have an aromatic functionality bonded directly to the imine N atoms. In both cases the emission extended from 500–700 nm and was independent of the excitation wavelength over a broad range beginning from about 250 nm and extending to 450 nm for compound **1** and to 500 nm for compound **2**. The excitation feature at ~280 nm occurred in all measured spectra and is an artefact due to the excitation correction in this region. The similarity of the luminescence properties of these compounds with each other and, for example, N-salicylidene-o-aminophenol (saph$H_2$) and its derivatives,[49] or salicylaldehyde azine[50] suggests that the salicylidene moiety primarily determines the spectral properties which are not strongly affected by the bonded biological directing functional groups. This is in contrast to a report for N-(pyrene)-salicylaldimine for which the luminescence properties were attributed to the strongly fluorescent pyrene moiety.[51] The luminescence intensity of compound **2** is much greater than compound **1** (shown magnified five times in Fig. 7 for clarity) and this is also reflected in the measured quantum yields being 3.9% for compound **1** but 17% for compound **2** when measured using an excitation wavelength of 390 nm. Although the quantum efficiencies of aromatic compounds can approach 100% for strong fluorophores, the value for compound **2** compares favourably to well-known anthracene (25%)[52] or aluminum-tris-quinolate ($Alq_3$) which is applied in organic LEDs (32%),[53] suggesting that it may be effective for biological imaging. For comparison, tryptophan is the most fluorescent naturally occurring amino acid and has a quantum yield of 13%.[54] The increased luminescence intensity and quantum yield of compound **2** relative to compound **1** must be attributed to the 3-amino-9-ethylcarbazole linked to the salicylaldehyde backbone. It is not thought that it contributes directly to the light emission (having an emission wavelength of ~400 nm[55]), but it may be more effective in stabilizing the entire molecule and reducing non-radiative recombination due to its large size or the carbazole group may be excited and effectively transfer energy to the salicylidene moiety.

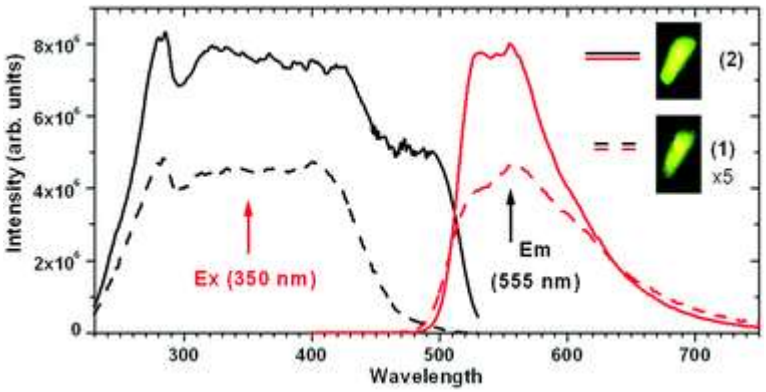


**Fig. 7** Photoluminescence excitation and emission spectra of the compounds **1** and **2**, including inset images of emission. The data for compound **1** have been multiplied five times for ease of comparison.

Fig. 8 compares the spectral properties of compounds **3**, **4** and **5** which all have a –$CH_2CH_2$–R chain bonded to the N atom of the salicylaldehyde backbone, where R = histamine, tryptamine and tyramine respectively. These compounds exhibited lower fluorescence than compounds **1** and **2** and the quantum yields were in the region of 1% or less (see Table 5). The peak emission wavelength (for excitation at 390 nm) varied from 555 nm for compound **3**, to 525 nm for compound **4** and 500 nm for compound **5**. This shift to shorter emission wavelength occurred together with a decrease in the width of the emission band and the

fluorescent colour of the compounds changed from yellow to green. Unlike for compounds **1** and **2** the emission spectra of compounds **3**, **4** and **5** was affected by the excitation wavelength and shifted to longer wavelengths as the excitation wavelength increased. This is attributed to self-absorption effects due to the significant overlap of the excitation and emission wavelengths. For the excitation spectra the feature at 280 nm is a correction artefact occurring in all the spectra. Compound **3** has clearly differentiated excitation peaks at 390 nm and 480 nm with the band extending well beyond 500 nm, while the excitation bands of compounds **4** and **5** have a range of approximately 250–480 nm. It is therefore clear that the biological groups bonded to the salicylidene moiety have a significant effect on the fluorescence properties in these compounds, although in general the quantum yields are poor for those containing the $–CH_2CH_2–R$ chain. Linking the salicylaldehyde backbone to the biological group using an ethylimino chain is therefore not recommended for biological imaging applications.

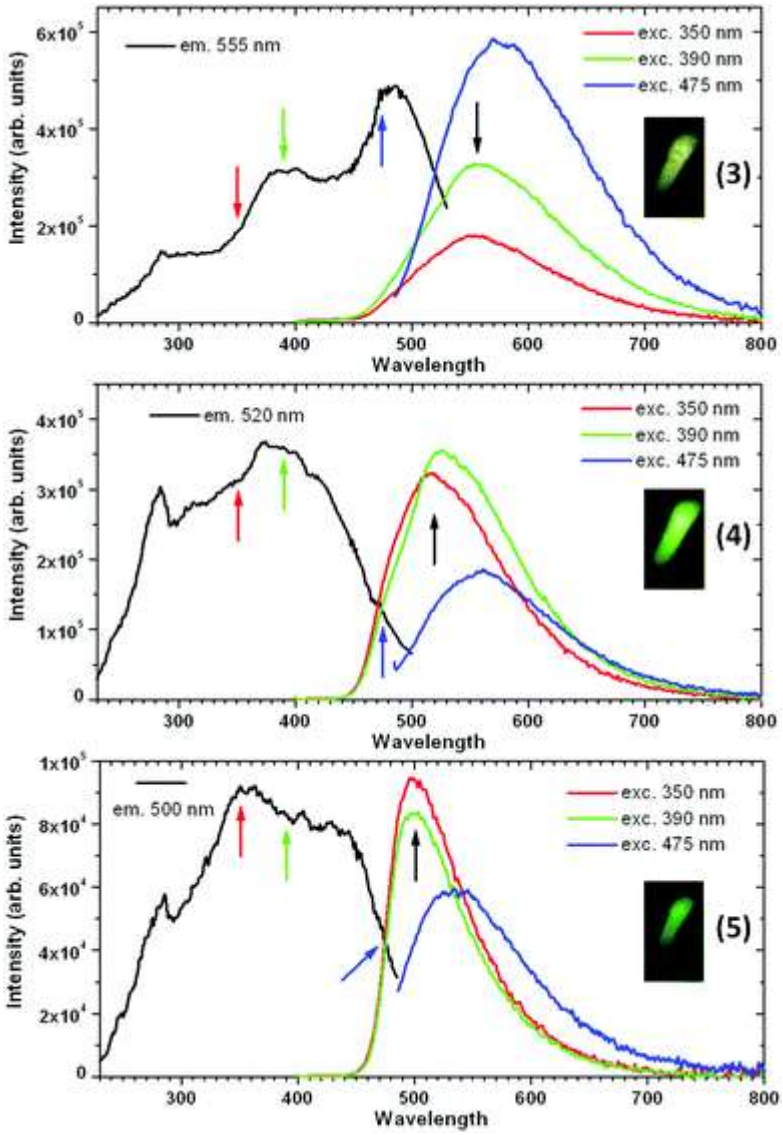


**Fig. 8** Photoluminescence excitation and emission spectra of the compounds **3**, **4** and **5**, including inset images of the emission.

**Table 5** Quantum yields of the compounds **1–5** excited at 280, 350, 390 and 480 nm. A comparison of relative quantum yields was obtainable at 390 nm

| | Quantum yield (%) | | | |
|---|---|---|---|---|
| **Compound** | **280 nm** | **350 nm** | **390 nm** | **480 nm** |
| **1** | 4.2 | | 3.9 | |
| **2** | 22 | | 17 | |
| **3** | | | 0.7 | 2.9 |
| **4** | 0.9 | | 1.3 | |
| **5** | | 0.2 | 0.2 | |

## 4. Conclusions

We report in this paper the development of five imino salicylidene-based bifunctional chelators which are intended to meet several criteria namely the ability to coordinate to a radiopharmaceutical synthon fac-$[M(CO)_3]^+$ (M = $^{188/186}$Re or $^{99m}$Tc); contain a biological directing molecule (i.e. 1,2,4-triazole, 3-amino-carbazole, histamine, tryptamine and tyramine) which may affect the chemotherapeutic or biological distribution of the compound in vivo and finally to act as a biological cellular imaging agent with distinct photoluminescent capability. Studies of such nature is critical as the addition of a 'biologically active' substituent does not guarantee any chemotherapeutic application of the final bifunctional chelator. However, the use of the functional groups with a known receptor binding is the starting point and utilised in research fields such as the structurally based Fragment Based Drug Design (FBDD) which examines specific protein–ligand binding of low-molecular-weight fragments to derive a model for possible drug-like lead compounds.[56–58] Radiopharmaceutical development, for which these chelators were designed, have two valuable pathways which can be exploited. The primary therapy/diagnostic source is naturally the radionuclide of interest, for example, rhenium-186/188 for therapy and technetium-99m for diagnosis. However the second less exploited method is designing a cytotoxic bifunctional chelator which results in radiopharmaceuticals which are chemotherapeutic as well as radiotherapeutic. One is then able to treat a disease site by two methods simultaneously. It is therefore critical that a basic understanding of the chemotherapeutic, photoluminescence, stability and suitability of both the chelator and radiopharmaceutical model be individually examined. The crystallographic studies adequately describe the solid-state orientation of the molecules while providing detailed suggestions to differences observed during DFT calculations. In vitro cancer cell testing indicates no chemotherapeutic application for these organic chelators on the basis of their own structure with no cell growth retardation for renal, melanoma or breast cancer cells. However these chelators have recently illustrated a future application as a model type for dinuclear theranostic development.[59] All of the chelators indicate luminescent capability with compound **2** being significantly luminescent with a quantum yield of 22% at 280 nm.

## Conflicts of interest

There are no conflicts of interest to declare.

**Acknowledgements**

Financial assistance from the University of the Free State is gratefully acknowledged. We thank SASOL, the South African National Research Foundation (Grant Number 99139, A Brink; Grant Number 93214, R. E. Kroon) and the University of the Free State Strategic Academic Cluster Initiative (Advanced Biomolecular Research and the Materials and Nanosciences Clusters) for financial support of this project.

**References**

1. S. Lui, Chem. Soc. Rev., 2004, 33, 445–461.
2. R. Alberto, R. Schibli, A. Egli, P. A. Schubiger, W. A. Herrmann, G. Artus, U. Abram and T. A. Kaden, J. Organomet. Chem., 1995, 493, 119–127.
3. R. Alberto, R. Schibli, A. P. Schubiger, U. Abram, H. J. Pietzsch and B. Johannsen, J. Am. Chem. Soc., 1999, 121, 6076–6077.
4. T. W. Spradua and J. A. Katzenellenbogen, Bioconjugate Chem., 1998, 9, 765–772.
5. M. M. Saw, P. Kurz, N. Agorastos, T. S. A. Hor, F. X. Sundram, Y. Kai Yan and R. Alberto, Inorg. Chim. Acta, 2006, 359, 4087–4094.
6. M. L. Biechlin, A. Bonmartin, F. N. Gilly, M. Fraysse and A. du Moulinet d'Hardemare, Nucl. Med. Biol., 2008, 35, 679–687.
7. L. Maria, S. Cunha, M. Videira, L. Gano, A. Paulo, I. C. Santos and I. Santos, Dalton Trans., 2007, 3010–3019.
8. K. Zelenka, L. Borsig and R. Alberto, Bioconjugate Chem., 2011, 22, 958–967.
9. M. Morais, B. L. Oliveira, J. D. G. Correia, M. C. Oliveira, M. A. Jiménez, I. Santos and P. D. Raposinho, J. Med. Chem., 2013, 56, 1961–1973.
10. S. Mundwiler, M. Kündig, K. Ortner and R. Alberto, Dalton Trans., 2004, 1320–1328.
11. J. M. Botha and A. Roodt, Met.-Based Drugs, 2008, 745989.
12. M. Schutte, G. Kemp, H. G. Visser and A. Roodt, Inorg. Chem., 2011, 50, 12486–12498.
13. A. Brink, H. G. Visser and A. Roodt, Inorg. Chem., 2013, 52, 8950–8961.
14. F. Zobi and B. Spingler, Inorg. Chem., 2012, 51, 1210–1212.
15. G. Santoro, O. Blacque and F. Zobi, Metallomics, 2012, 4, 253–259.
16. A. Brink and J. R. Helliwell, IUCrJ, 2017, 4, 283–290.
17. J. Clayden, N. Greeves, S. Warren and P. Wothers, Organic Chemistry, Oxford University Press, Oxford, 2001.
18. M. S. Burstone, Enzyme Histochemistry, Academic Press, New York, 1962.
19. E. C. Stack, C. Wang, K. A. Roman and C. C. Hoyt, Methods, 2014, 70, 46–58.
20. R. B. Silverman, The Organic Chemistry of Drug Design and Drug Action, Elsevier Academic Press, London, 2nd edn, 2004.
21. A. L. Nicely and J. M. Lisy, J. Phys. Chem. A, 2011, 115, 2669–2678.
22. T. Nogrady and D. F. Weaver, Medicinal Chemistry: A Molecular and Biochemical Approach, Oxford University Press, Inc., Oxford, 3rd edn, 2005.
23. Bruker, APEX2 (Version 1.0-27). Bruker AXS Inc., Madison, Wisconsin, USA, 2005.
24. Bruker, COSMO (Version 1.48). Bruker AXS Inc., Madison, Wisconsin, USA, 2003.
25. Bruker, SAINT-Plus (Version 7.12) (including XPREP). Bruker AXS Inc., Madison, Wisconsin, USA, 2004.
26. Bruker, SADABS (Version 2004/1). Bruker AXS Inc., Madison, Wisconsin, USA, 1998.

27. A. Altomare, M. C. Burla, M. Camalli, G. L. Cascarano, C. Giacovazzo, A. Guagliardi, A. G. G. Moliterni, G. Polidori and R. Spagna, J. Appl. Crystallogr., 1999, 32, 115–119.
28. L. J. Farrugia, J. Appl. Crystallogr., 1999, 32, 837–838.
29. G. M. Sheldrick, SHELXL97, Program for Solving Crystal Structures, University of Göttingen, Germany, 1997.
30. K. Brandenburg and H. Putz, DIAMOND, Release 3.0c, Crystal Impact GbR, Bonn, Germany, 2005.
31. Hyperchem™ Release 7.52, Windows Molecular Modeling System, Hypercube, Inc., 2002.
32. M. J. Frisch, G. W. Trucks, H. B. Schlegel, G. E. Scuseria, M. A. Robb, J. R. Cheeseman, J. A. Montgomery Jr., T. Vreven, K. N. Kudin, J. C. Burant, J. M. Millam, S. S. Iyengar, J. Tomasi, V. Barone, B. Mennucci, M. Cossi, G. Scalmani, N. Rega, G. A. Petersson, H. Nakatsuji, M. Hada, M. Ehara, K. Toyota, R. Fukuda, J. Hasegawa, M. Ishida, T. Nakajima, Y. Honda, O. Kitao, H. Nakai, M. Klene, X. Li, J. E. Knox, H. P. Hratchian, J. B. Cross, V. Bakken, C. Adamo, J. Jaramillo, R. Gomperts, R. E. Stratmann, O. Yazyev, A. J. Austin, R. Cammi, C. Pomelli, J. W. Ochterski, P. Y. Ayala, K. Morokuma, G. A. Voth, P. Salvador, J. J. Dannenberg, V. G. Zakrzewski, S. Dapprich, A. D. Daniels, M. C. Strain, O. Farkas, D. K. Malick, A. D. Rabuck, F. Raghavachari, J. B. Foresman, J. V. Ortiz, Q. Cui, A. G. Baboul, S. Clifford, J. Cioslowski, B. B. Stefanov, G. Liu, A. Liashenko, P. Piskorz, I. Komaromi, R. L. Martin, D. J. Fox, T. Keith, M. A. Al-Laham, C. Y. Peng, A. Nanayakkara, M. Challacombe, P. M. W. Gill, B. Johnson, W. Chen, M. W. Wong, C. Gonzalez and J. A. Pople, Gaussian-03, Revision C.01, Gaussian, Inc., Wallingford, CT, 2004.
33. A. D. Becke, J. Chem. Phys., 2003, 98, 5648–5652.
34. P. C. Hariharan and J. A. Pople, Theor. Chim. Acta, 1973, 28, 213–222.
35. M. M. Francl, W. J. Petro, W. J. Hehre, J. S. Binkley, M. S. Gordon, D. J. De Free and J. A. Pople, J. Chem. Phys., 1982, 77, 3654–3665.
36. N. Kolesnikova and H. Hoppe, CSIR Biosciences Pharmacology Group, In vitro Cancer Screening Report, South Africa, reported 2011-01-17.
37. N. Kolesnikova, D. Koot and H. Hoppe, CSIR Biosciences Pharmacology Group, In vitro Cancer Screening Report, South Africa, reported 2011-07-19.
38. R. B. Silverman, The Organic Chemistry of Drug Design and Drug Action, Elsevier Academic Press, London, 2nd edn, 2004.
39. M. S. Burstone, Enzyme Histochemistry, Academic Press, New York, 1962.
40. A. L. Nicely and J. M. Lisy, J. Phys. Chem. A, 2011, 115, 2669–2678.
41. J. Clayden, N. Greeves, S. Warren and P. Wothers, Organic Chemistry, Oxford University Press, Oxford, 2001.
42. E. Tozzo, S. Romera, M. P. dos Santos, M. Muraro, R. H. de, A. Santos, L. M. Lião, L. Vizotto and E. R. Dockal, J. Mol. Struct., 2008, 879, 110–120.
43. A. Brink, H. G. Visser and A. Roodt, J. Coord. Chem., 2011, 64, 122–133.
44. F. Arod, P. Pattison, K. J. Schenk and G. Chapuis, Cryst. Growth Des., 2007, 7, 1679–1685.
45. A. Brink, H. G. Visser and A. Roodt, Inorg. Chem., 2014, 53, 12480–12488.
46. T. D. Marake, P. P. Mokolokolo, H. G. Visser and A. Brink, Acta Crystallogr., 2015, C71, 423–429.
47. A. Brink, H. G. Visser and A. Roodt, Polyhedron, 2013, 52, 416–423.
48. P. Skehan, R. Storeng, D. Scudiero, A. Monks, J. McMahon, D. Vistica, J. T. Warren, H. Bokesch, S. Kenney and M. R. Boyd, J. Natl. Cancer Inst., 1990, 82, 1107.

49. A. Kagkelari, V. Bekiari, E. Stathatos, G. S. Papaefstathiou, C. P. Raptopoulou, T. F. Zafiropoulos and P. Lianos, J. Lumin., 2009, 129, 578–583.
50. J. Yang, J. Rui, X. Xu, Y. Yang, J. Su, H. Xu, Y. Wang, N. Sun and S. Wang, RSC Adv., 2016, 6, 30636–30641.
51. I. Yilmaz, Transition Met. Chem., 2008, 33, 259–265.
52. F. P. Schwarz and S. P. Wasik, Anal. Chem., 1976, 48, 524–528.
53. D. Z. Garbuzov, V. Bulović, P. E. Burrows and S. R. Forrest, Chem. Phys. Lett., 1996, 249, 433–437.
54. L. D. Lavis and R. T. Raines, ACS Chem. Biol., 2008, 3, 142–155.
55. S. Z. Tan, Y.-J. Hu, F.-C. Gong, Z. Cao, J.-Y. Xia and L. Zhang, Anal. Chim. Acta, 2009, 636, 205–209.
56. D. Joseph-McCarthy, A. J. Campbell, G. Kern and D. Moustakas, J. Chem. Inf. Model., 2014, 54, 693–704.
57. D. A. Erlanson, Top. Curr. Chem., 2012, 317, 1–32.
58. C. W. Murray, M. L. Verdonk and D. C. Rees, Trends Pharmacol. Sci., 2012, 33, 224–232.
59. P. P. Mokolokolo, A. Frei, M. S. Tsosane, D. V. Kama, M. Schutte-Smith, A. Brink, H. G. Visser, G. Meola, R. Alberto and A. Roodt, Inorg. Chim. Acta, 2018, 471, 249–256.